Accuracy of Interstitial Iron Measurements on P-Type Multicrystalline Silicon Blocks by Quasi-Steady-State Photoconductance

Mohsen Goodarzi, Ronald A. Sinton, Hao Jin, Peiting Zheng, Wei Chen, Quanzhi Wang, and Daniel Macdonald

Abstract—A detailed knowledge of the distributions of carrier lifetimes, impurities, and crystal defects in silicon ingots is key for understanding and improving wafer quality, as well as solar cell processing steps. In this work, we have validated the use of the quasi-steady-state photoconductance method on p-type multicrystalline silicon blocks to determine the interstitial iron concentration. The extracted iron concentrations along a silicon block were compared with the interstitial iron concentrations measured on wafers from different heights of an adjacent block. The lifetime measurements were performed on the block before and after flashing to break the iron–boron pairs. The impact of nonuniform carrier profiles during the block measurements on the extraction of the Fe profiles is discussed and quantified based on simulations of the quasi-steady-state measurement conditions. The simulation results reveal a slight error in the extracted interstitial iron concentration along the block. However, this error is generally less than 20% for iron concentrations below 10^{11} cm^{-3}, which is typical in the central region of an ingot, and in any case, can be corrected for based on the modeling results.

Index Terms—Carrier lifetime, iron concentration, quasi-steady-state photoconductance (QSSPC), silicon block.

I. INTRODUCTION

THE quasi-steady-state photoconductance (QSSPC) method is well established for the measurement of minority carrier lifetimes on silicon wafers [1]. Due to its advantages in early-stage characterization, the method has also been recently applied to ingot and block lifetime measurements and characterization of crystal defects and impurities in them. Particularly, the interstitial iron concentration has been studied [2], [3] because of its important role in limiting the minority carrier lifetime in multicrystalline silicon ingots prior to cell processing. This application can provide more immediate feedback on crystal growth quality through specific knowledge about the impurities and crystal defects in the ingots and blocks. Consequently, more reliable decisions can be made for cropping ingots and blocks for wafering purposes. It may also be possible to sort the wafers at the start of processing and tune the cell process for different quality wafers coming from the different sections of the block [4]. This detailed information can potentially be used during the manufacturing processes to achieve higher efficiency as well as higher yield. Some recent examples of characterization methods capable of providing such information at the ingot level are the QSSPC instrument [5], which is used in this work, and Photoluminescence (PL)-based methods for ingot characterization [6], [7]. There have also been studies investigating the effect of surface recombination velocity (SRV) and sample thickness on the excess minority carrier lifetime in silicon wafers and blocks using a dynamic photoluminescence approach [8], [9]. It has also been shown that a high SRV can introduce large deviations between the measured and actual bulk lifetime [4], [5], [10].

However, there have not been studies on the accuracy of the QSSPC block method when used to determine the interstitial iron concentration. Thus, this study is focused on validating the accuracy of the extracted interstitial iron concentration [Fe$_i$] from QSSPC measurements on p-type multicrystalline silicon blocks, through a comparison between the extracted [Fe$_i$] values on a block and the interstitial iron measured on wafers from an adjacent block. A simulation tool was developed to model the QSSPC lifetime measurement in the block before and after breaking Fe–B pairs [11]. The main source of potential errors is the nonuniform excess carrier densities which are always present in ingot measurements, in contrast to the typical conditions during the lifetime measurement on a wafer. (We note that previous studies [12] have investigated the impact of such nonuniform carrier profiles on the measurement of interstitial iron in low lifetime wafers, but were not targeted specifically at measurements at the ingot level.) In this work, we use such modeling to show that the [Fe$_i$] data are only slightly affected by the nonuniform carrier profiles in most practical cases, and that extracted [Fe$_i$] data from measurements on a p-type multicrystalline silicon brick agree well with wafer-based measurements from an adjacent brick. A correction procedure is also presented for reducing the relatively small error in the ingot-based [Fe$_i$] data taking into account the effects of the doping, the average

M. Goodarzi and D. Macdonald are with the Research School of Engineering, The Australian National University, Canberra, ACT 2601, Australia (e-mail: Mohsen.goodarzi@anu.edu.au; daniel.macdonald@anu.edu.au).

R. A. Sinton is with the Sinton Instruments Inc., Boulder, CO 80301 USA (e-mail: ron@sintoninstruments.com).

H. Jin, P. Zheng, W. Chen, and Q. Wang are with the JinkoSolar, Shangrao 334100, China (e-mail: hao.jin@jinkosolar.com; peiting.zheng@jinkosolar.com; wei.chen@jinkosolar.com; quanzhi.wang@jinkosolar.com).

Color versions of one or more of the figures in this paper are available online at http://ieeexplore.ieee.org.

Digital Object Identifier 10.1109/JPHOTOV.2017.2716785

injection level, and the background lifetime due to all other bulk recombination channels except for Fe_i.

II. SIMULATION OF QSSPC MEASUREMENTS

The excess carrier profiles under steady-state conditions are simulated numerically in this work. A "BCT-400" measurement system from Sinton Instruments is used in this work and the aim is to simulate how the measurements are performed by the tool.

Below we show how the simulation model was developed, and then describe how the effective carrier lifetime was calculated. A transfer function is then applied to the effective lifetime ($\tau_{QSS-eff}$) in order to eliminate the effect of the high SRV due to the unpassivated as-cut surface. This results in an estimated QSS bulk lifetime ($\tau_{QSS-bulk}$). The transfer function used in this work is specific to the BCT-400 tool, but in general other transfer functions could be applied. The bulk lifetime is simulated before and after the dissociation of Fe–B pairs and the results are used to determine the interstitial iron concentration in silicon blocks. The accuracy of the extracted $[Fe_i]$ and the impact of several factors such as doping and the average injection level are also addressed at the end of this section.

Steady-state conditions require that the total rates of electron–hole pair generation and recombination are equal across the entire sample, although they may not be equal locally. This means that

$$\tau_{QSS-eff} = \frac{\Delta n W}{g_{cum}} \quad (1)$$

where $\tau_{QSS-eff}$ is the QSS effective lifetime including recombination in the bulk as well as the surface, Δn is the excess carrier density, W is the sample thickness, and g_{cum} is the areal carrier generation rate (cm^{-2}) over the entire thickness [not to be confused with the conventional volume generation rate, G (cm^{-3})], which can be calculated from the generation profile of the light source. It should be noted that in typical cases where the minority carrier diffusion length is significantly larger than the sample thickness, such as for measurements on passivated wafers, Δn can be assumed to be constant across the sample, and will be a single value at a given light intensity.

The photoconductance measurements monitor the increase in the sample conductivity σ due to illumination. The excess carrier density can be calculated by

$$\Delta n = \frac{\Delta \sigma}{q \left(\mu_n + \mu_p \right) W} \quad (2)$$

where μ_n and μ_p are the electron and hole mobility, respectively. The mobility is a slowly varying function of the carrier density so requires an initial approximation of the Δn value, followed by an iterative procedure in order to convert the photoconductance into carrier densities using (2) [4].

Cuevas [13] proposed a model to simulate QSS conditions in silicon wafers, utilizing numerical analysis in order to find Δn for a given thickness, W, and ultimately find $\tau_{QSS-eff}$ from (1). In the method, the sample thickness was divided into intervals Δx small enough to ensure the electron current across the Δx thickness can be considered constant. As described in detail in [13], numerical analysis involves equating the total

generation and total recombination of excess minority carriers across the sample thickness (W) as well as numerically solving the continuity equation in each element (Δx thick), including the diffusion of carriers into and out of the elements. In this work, a quasi-infinite SRV of order of $10^6 \, cm \cdot s^{-1}$ [14], [15] was assumed, as a consequence of the nonpassivated surface on an as-cut block. However, this high recombination velocity will introduce a large deviation between the measured effective lifetime including the effect of high SRV ($\tau_{QSS-eff}$) and actual bulk lifetime excluding high SRV effect, as discussed in [8]. In our simulation tool, a transfer function as defined in [4] is implemented to convert simulated effective QSS lifetimes into an estimated bulk lifetimes ($\tau_{QSS-bulk}$).

A significant challenge in applying the QSSPC technique to a block is its large depth (thickness) which can be considered as infinite in comparison to the minority carrier diffusion length. As a result, the Δn profile in a block is never uniform, and so an average value is required for the data analysis. A weighted average excess carrier density Δn_{avg} and effective thickness W_{eff} were introduced by Bowden and Sinton [4] to address these problems:

$$\Delta n_{avg} = \frac{\int_0^\infty \Delta n^2 dx}{\int_0^\infty \Delta n dx} \quad W_{eff} = \frac{\left(\int_0^\infty \Delta n dx \right)^2}{\int_0^\infty \Delta n^2 dx}. \quad (3)$$

The thickness value has to be moderated by the tool's coil depth sensitivity, which in this case is less than 3 mm. Full details about the coil depth sensitivity profile are discussed in [15]. The sensitivity function in [15] is applied to the simulated excess carrier profile to model the profile that the BCT-400 uses to measure the effective lifetime.

Since we are interested in extracting the dissolved iron concentration $[Fe_i]$ in this work, the bulk lifetime may be expressed in terms of the following components:

$$\frac{1}{\tau_{bulk}} = \frac{1}{\tau_{Fe_i}} + \frac{1}{\tau_{Auger}} + \frac{1}{\tau_{other}} \quad (4)$$

where τ_{Fe_i} is the lifetime due to the dissolved Fe, τ_{Auger} is the intrinsic lifetime (Auger and radiative) [16], and τ_{other} represents all other bulk recombination channels such as dislocations and grain boundaries (GBs), and is considered to be injection independent in this work.

The simulation model allows for various Fe_i or Fe–B concentrations as well as other inputs such as the doping concentration and τ_{other} to simulate the carrier profiles and extracted lifetimes.

Zoth and Bergholz [17] showed that the interstitial iron concentration in silicon can be calculated from

$$[Fe_i] = C \left(\frac{1}{\tau_1} - \frac{1}{\tau_0} \right) \quad (5)$$

where τ_0 and τ_1 are the bulk lifetimes measured at a fixed injection level before and after breaking Fe–B pairs, respectively.

The Fe_i concentration and factor C have been calculated using the method developed in [11] and the recombination parameters (energy levels, capture cross sections, and the thermal velocity) from [18] for $\Delta n = 10^{15} \, cm^{-3}$.

Fig. 1(a) illustrates an example of a volume generation profile G (cm^{-3}), as well as carrier density as a function of the
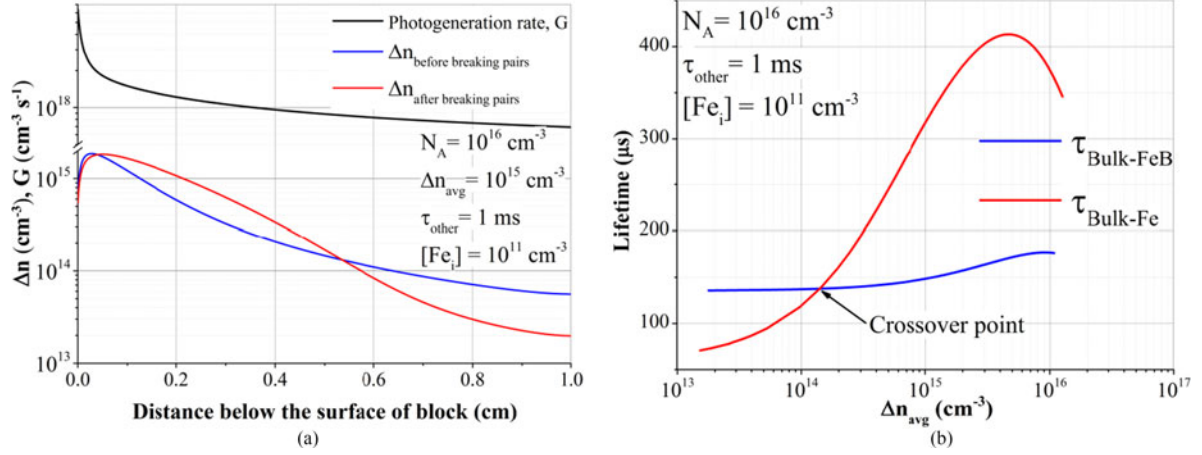
Fig. 1. (a) Simulated excess carrier density (before and after breaking Fe–B pairs) and volume photogeneration rate G versus distance below the block surface. (b) Simulated extracted QSSPC bulk lifetime as a function of the average excess carrier density before and after breaking the Fe–B pairs: the crossover point is located at an excess carrier density just above 10^{14} cm^{-3}.

block depth, for a doping concentration of 10^{16} cm^{-3}, an average excess carrier density of 10^{15} cm^{-3}, and a τ_{other} value of 1 ms. The crossover point due to the presence of Fe–B pairs can be observed a little above $\Delta n = 10^{14}$ cm^{-3}. This is related to the crossover point observed in typical lifetime versus injection level data measured on wafers [19]. In general, the position of the crossover point may vary in an ingot measurement, due to the impact of diffusion currents resulting from the nonuniform carrier densities, and because of the approximate nature of the effective width and average excess carrier density definitions. However, in many practical cases, the crossover point occurs close to where it is expected based on the Shockley–Read–Hall parameters, as indicated in Fig. 1(b), which plots the simulated extracted QSSPC bulk lifetime as a function of the average excess carrier density before and after breaking the Fe–B pairs.

The importance of accurate approximations of Δn_{avg} and W_{eff} is that they are used to calculate the minority carrier lifetime which will later be used to extract $[\text{Fe}_i]$. Hence, the model and the simulation tool were used to validate the accuracy of the measured interstitial iron concentration. This was performed by varying the $[\text{Fe}_i]$, Δn_{avg}, doping, and τ_{other}, all of which can affect the results. The error in the resulting $[\text{Fe}_i]$ was defined as

$$\text{Error} = \frac{[\text{Fe}_i]_{\text{Calculated}} - [\text{Fe}_i]_{\text{Actual}}}{[\text{Fe}_i]_{\text{Calculated}}} \qquad (6)$$

where $[\text{Fe}_i]_{\text{Calculated}}$ is calculated from (5) with the simulated lifetime before and after breaking the Fe–B pairs and $[\text{Fe}_i]_{\text{Actual}}$ is the input value of the iron concentration used in the model.

The simulations revealed that the main source of error is the iron concentration itself (see Fig. 2), which reduces the diffusion length as it increases. However, the overestimation error (positive values) decreased as the iron concentration increased toward 10^{11} cm^{-3}, then the error becomes negative, indicating an increasing underestimation of the interstitial iron concentration. In all cases, the error was less than –50% (when $N_A = 10^{16}$ cm^{-3} and $\tau_{\text{other}} = 300 \,\mu\text{s}$) for iron concentrations below 10^{12} cm^{-3}, which is well above the upper limit observed in the central part of typical multicrystalline bricks.
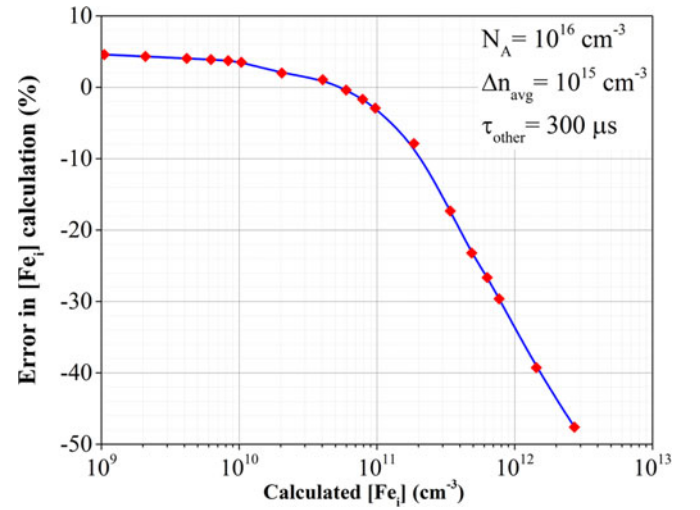

Fig. 2. Effect of interstitial iron concentration on the $[\text{Fe}_i]$ calculation error.

The chosen value of Δn_{avg} at which the effective lifetimes are extracted also affects the accuracy of the calculation, as shown in Fig. 3. In order to avoid the impact of the crossover point on the lifetime measurements, the simulation did not include Δn_{avg} values between 5×10^{13} and 5×10^{14} cm^{-3}. The results illustrate that selecting $\Delta n_{\text{avg}} = 10^{15}$ cm^{-3} for measuring Fe$_i$ concentrations is a reasonable choice, and introduces similar or less error than injection levels below the crossover point, while avoiding the adverse effects of minority carrier trapping.

The value of τ_{other} was also found to impact the accuracy of the extracted $[\text{Fe}_i]$ values, as shown in Fig. 4 for a doping concentration of 10^{16} cm^{-3}. For values of τ_{other} under about 200 μs, it generally caused an underestimation of $[\text{Fe}_i]$, while for higher values of τ_{other}, it initially causes an overestimation for lower $[\text{Fe}_i]$ values, and then an increasing underestimation for higher $[\text{Fe}_i]$ values. It should be noted that when the bulk lifetime is limited by bulk recombination centers other than Fe$_i$ ($\tau_{\text{other}} < 200 \,\mu\text{s}$ and $[\text{Fe}_i] < 10^{11}$ cm^{-3}), changes in
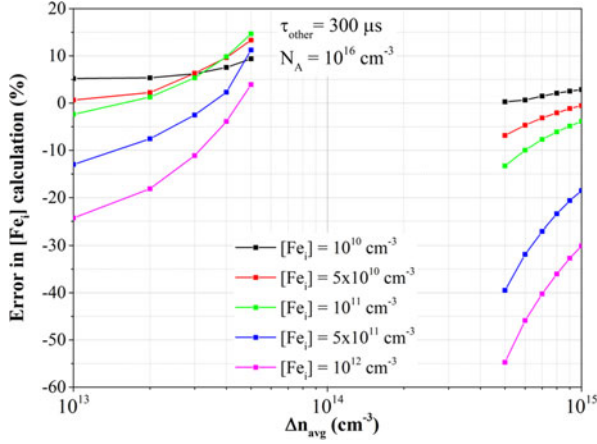
Fig. 3. Effect of injection level on the $[\text{Fe}_i]$ calculation error for various $[\text{Fe}_i]$ concentrations. Values in the range $\Delta n_{\text{avg}} = 5 \times 10^{13}$ to $5 \times 10^{14}\,\text{cm}^{-3}$ were excluded due to the impact of the crossover point.
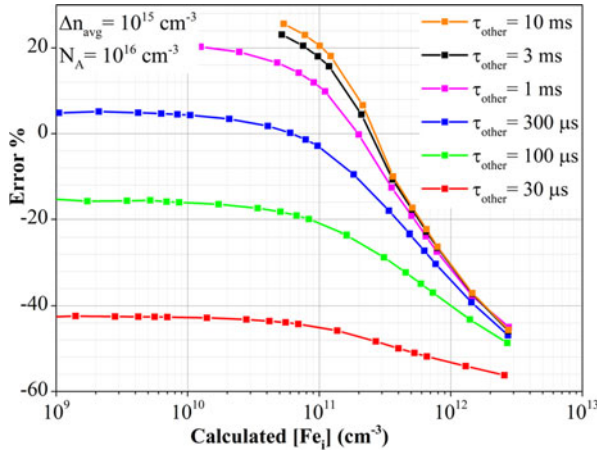

Fig. 4. Effect of τ_{other} on the $[\text{Fe}_i]$ calculation error as a function of $[\text{Fe}_i]$ for $N_A = 10^{16}\,\text{cm}^{-3}$.

the interstitial iron concentration do not affect the $[\text{Fe}_i]$ calculation error.

The decreasing trend in the error in Fig. 2 is the result of a combination of effects, such as the use of a single value of Δn_{avg} as defined in (3) to replace a range of Δn over the entire depth of W in (2), which itself is replaced by W_{eff}, the accuracy of the value of C in (5), which is strictly only valid for $\Delta n = 10^{15}\,\text{cm}^{-3}$, and the fact that the transfer function is not entirely accurate in converting the effective lifetime into the bulk lifetime.

The curves for the higher values of τ_{other} are truncated for the lower $[\text{Fe}_i]$ values, as in these cases the bulk lifetime becomes greater than 500 μs, meaning that the quasi-static assumption becomes increasingly invalid, and the transient lifetime method should be used. The relative uncertainties in transient and quasi-static lifetime measurements on blocks will be the subject of future work.

More figures for the Fe concentration error, with different values of N_A, are presented in the Appendix. These allow $[\text{Fe}_i]$ measurements with the Sinton BCT-400 tool to be corrected for the effects of nonuniform injection levels.
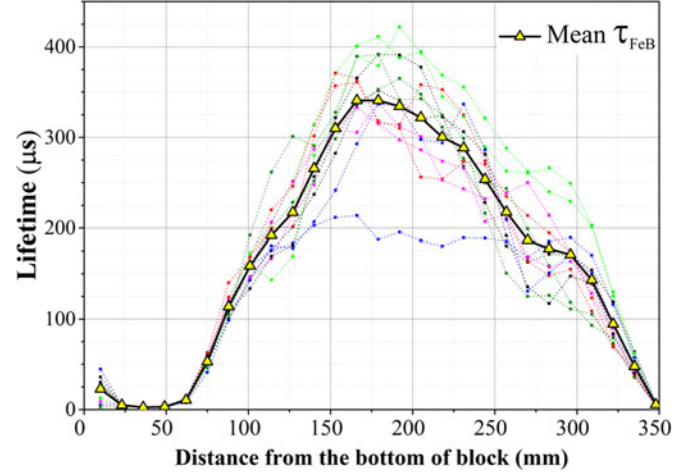

Fig. 5. QSSPC bulk lifetime versus block position before breaking Fe–B pairs. The dotted lines represent the lifetime from 12 scans on the four sides of the block and the solid line represents the mean value of those 12 scans.

III. EXPERIMENTAL METHODS

In this section, QSSPC lifetime measurements were performed on a standard multicrystalline silicon block grown at Jinko Solar, as well as on multiple wafers cut from an adjacent block, both before and after breaking Fe–B pairs, using a boule tester and a standard wafer lifetime tester, respectively. The data are used to extract interstitial iron concentrations on the block and the wafers to allow an assessment of the accuracy of the block measurements.

QSSPC measurements on the block were performed with a BCT-400 measurement system from Sinton Instruments, in QSSPC mode with a 1000-nm IR-Pass Schott glass filter. The sample was an uncropped rectangular block cut from the central part of a standard industrial G6 p-type multicrystalline silicon ingot, with a square base of 156 × 156 mm and a height of 367 mm. There were 28 QSSPC measurement points starting at 10 mm from the bottom edge up to 10 mm from the top edge with a 13 mm gap between each point.

The flash power was set to 400 WS with a 300 sun peak intensity and a 3.8 ms decay constant in all the measurements in this work. The lifetime evaluation started several milliseconds after the flash peak to eliminate initial decay modes. We note that the assumption of steady-state conditions for the QSSPC technique is only valid for bulk lifetimes much shorter than the flash decay time constant, meaning that bulk lifetimes <400 μs can be measured with reasonable accuracy. For longer lifetimes, dynamic changes in the carrier densities occur during the flash decay which are not accounted for under the QSS approximation. In such cases, transient measurements are recommended.

A total of fourteen 50 × 50 mm pieces were cut out of nine 156 × 156 mm wafers from different heights of the adjacent block and were passivated with PECVD SiN films on both surfaces. The interstitial iron concentration at a given height is assumed to be equal on adjacent bricks. This enabled us to use $[\text{Fe}_i]$ values extracted from lifetime measurements on the wafers (as a well-established reliable method) as a benchmark for validating the
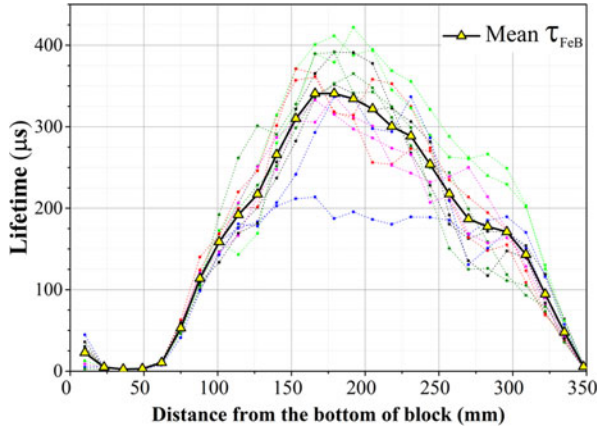
Fig. 6.   QSSPC bulk lifetime versus block position after breaking Fe–B pairs with illumination (red line with triangle data points) which is generally higher than the mean lifetime before breaking pairs (black line with square data points). The dotted lines represent the lifetime from 12 scans on the four sides of the block after breaking Fe–B pairs.
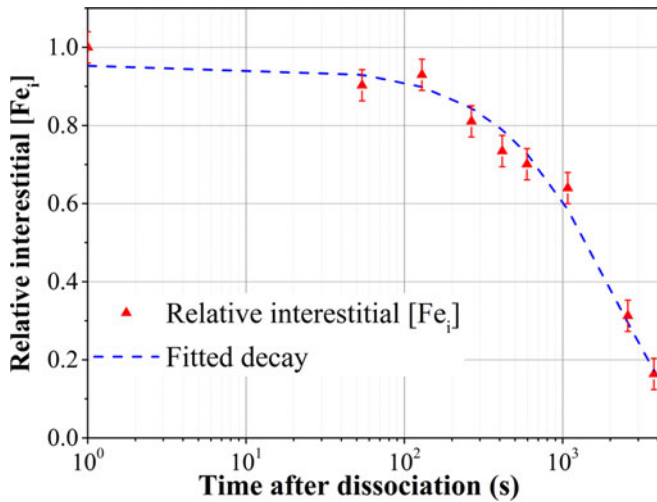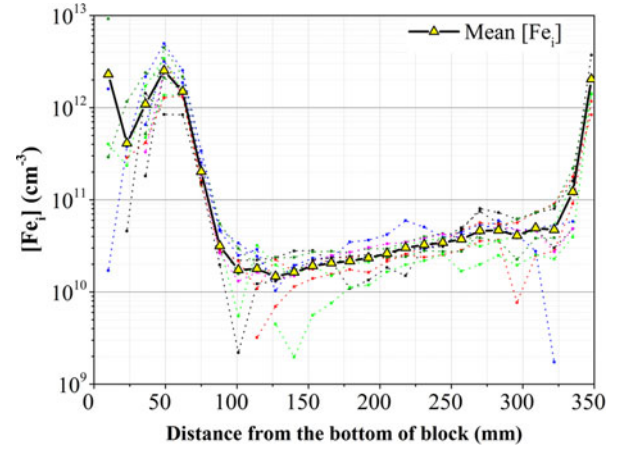

Fig. 8.   Extracted $[Fe_i]$ versus block position. The dotted lines represent the $[Fe_i]$ on 12 columns on the four sides of the block and the solid line represents the mean value of those 12 at each point.

Fig. 7.   Fe–B repairing as a function of time, after breaking the Fe–B pairs. The error bars were obtained from the 4% uncertainty in lifetime of the bulk samples as reported in [22]. The repairing time extracted from the fitted decay was 25 min, approximately equal to the expected value which was calculated based on the doping and temperature (23 min).
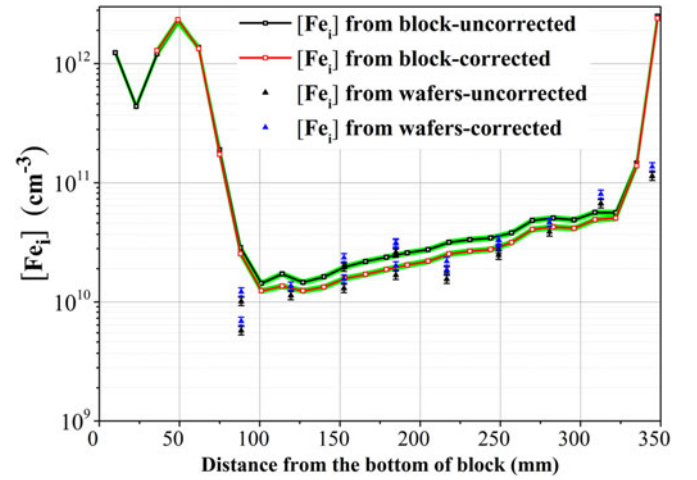

Fig. 9.   Average $[Fe_i]$ from the block before and after correcting for nonuniform carrier profiles, and the $[Fe_i]$ from the wafers before and after correcting for SiN gettering. The error shadow on the block $[Fe_i]$ data is 4%, and the error bars on the wafer data are 8% uncertainty of the transient lifetime data as reported in [22].

IV. RESULTS AND DISCUSSION

A. Lifetime Measurements on the Block

The carrier lifetime measurements were extracted at an average excess carrier density of $\Delta n = 10^{15} \, cm^{-3}$. Fig. 5 illustrates the bulk minority carrier lifetime, after applying the transfer function, in the block before breaking the Fe–B pairs as a function of block height. Each side of the block was divided into three columns where the lifetime tester was moved along each column from bottom to top to ensure the maximum possible area of each side was scanned. This resulted in measurements for a total of 12 different columns on 4 sides of the block shown in Fig. 5 (dotted lines). The large variations from scan to scan are due to the presence of inhomogeneously distributed crystallographic defects, such as GBs and dislocation clusters.

There was a band close to the bottom of the block where the lifetime was very low due to small grains and high levels of

block extracted $[Fe_i]$. The lifetime measurements on wafers were performed by a WCT-120 standard lifetime tester from Sinton Instruments using the transient method.

Multiple flashes with a Broncolor Picolite flash with a peak power of 1600 W were used in order to break the Fe–B pairs in the brick and the wafers. It has been shown that this method of breaking Fe–B pairs can achieve up to 99% dissociation in ingots for lifetimes above 5 μs [20]. The sample temperature was monitored by an IR camera during breaking the pairs and the change in temperature did not exceed 2 °C in the block and the wafers.
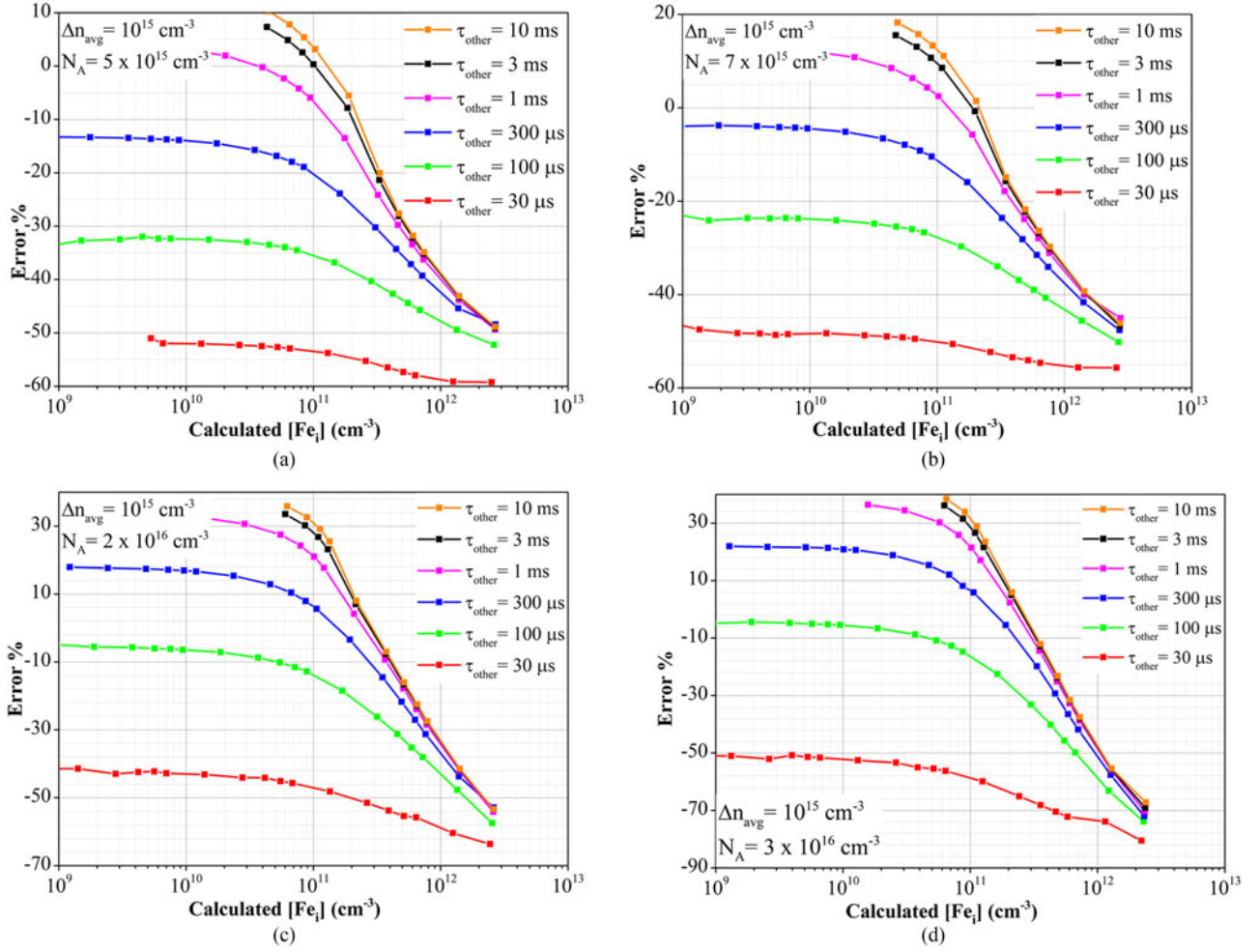
Fig. 10. The effect of τ_{other} on the $[\text{Fe}_i]$ calculation error for (a) $N_A = 5 \times 10^{15}$ cm^{-3}, (b) $N_A = 7 \times 10^{15}$ cm^{-3}, (c) $N_A = 2 \times 10^{16}$ cm^{-3}, and (d) $N_A = 3 \times 10^{16}$ cm^{-3}.

contamination. This region is normally cropped from the ingot before wafering.

The minority carrier lifetime (τ_{Fe_i}) was measured again after breaking the Fe–B pairs using the strong flash mentioned above.

As shown in Fig. 6, there was a general increase in the lifetime after breaking the pairs, as is expected since the measurements were performed at $\Delta n = 10^{15}$ cm^{-3} which is above the crossover point [11].

B. Fe Calculation From Lifetime Measurements

Prior to further analysis of the lifetime data, we first confirm that the observed changes in the carrier lifetimes after flashing are indeed due to the presence of dissolved iron. Then, the extracted $[\text{Fe}_i]$ data from the block were corrected according to the simulation results presented above, and then compared with the measured $[\text{Fe}_i]$ data from the wafers.

In order to confirm that the differences between the lifetime before and after flashing the sample are due to breaking Fe–B pairs (presence of dissolved iron), the sample was left in dark to allow the Fe–B pairs to reform. Several lifetime measurements were performed during this relaxation period. It has been shown in [11] that such lifetime data exponentially decay at a

rate of $1/\tau_{\text{assoc}}$ (where τ_{assoc} is the association time) for wafers containing interstitial iron. The same approach can be used for ingot measurements, in principle. The results are illustrated in Fig. 7 for one set of measurement points on the ingot. Tan *et al.* [21] showed the relationship between the Fe–B pair association time and the dopant density and temperature can be expressed as

$$\tau_{\text{assoc}} = \frac{5.7 \times 10^5}{N_A} T \exp \frac{0.66}{kT}. \tag{7}$$

Using the known dopant density (as determined from the dark conductance) of 8×10^{15} cm^{-3} and the ingot temperature (308 K) results in an expected Fe–B pair formation time of approximately 23 min. This compares well with the measured repairing time of 25 min extracted from fitting our lifetime data in Fig. 7. This confirms that the changes in lifetime we have observed are indeed due to the presence of interstitial iron.

The extracted interstitial iron concentrations along the block are shown in Fig. 8. The values were calculated from (5) with the method developed by Macdonald *et al.* [11], including the impact of the doping density variation along the block. As can be seen, the interstitial iron concentration first rapidly decreases

along the growth direction from the bottom of the ingot, and then displays a steady increase in the middle of the ingot with a final rapid increase at the top of the block. Such a trend has earlier been reported by numerous authors, for example, Sinton *et al.* [5] and Mitchell *et al.* [20], and can be explained by solid-state in-diffusion of Fe from the crucible, and impurity segregation into the liquid phase during crystallization, respectively. It is also notable that the extracted $[\text{Fe}_i]$ data on different sides of the block are less scattered in comparison with the lifetime data mentioned above. This indicates that our assumption of an almost equal dissolved iron concentration in adjacent central bricks is reasonable.

C. Block Versus Wafers Results

Fig. 9 presents the measured interstitial iron concentration of 14 wafers from different heights of the central part of an adjacent block (wafers were not sawn from near the bottom and top of the block as these are routinely cropped prior to wafering).

Liu *et al.* [23] have recently shown that the interstitial iron concentration decreases during the deposition of SiN by PECVD, due to gettering of Fe_i to the SiN films. The $[\text{Fe}_i]$ reduction in the samples due to the gettering effect was estimated using the model in [23] and found to be approximately 20% for the SiN deposition conditions used in this work (deposition temperature of 250 °C for a total time of 30 min). The corrected wafer values are also shown in Fig. 9, representing the expected $[\text{Fe}_i]$ values in the as-cut wafers. As shown, there is a steady increase in the interstitial iron concentration with increasing ingot height, in agreement with the data measured on the block. The error bars for the wafer data at each point were calculated assuming an 8% uncertainty in the transient lifetime measurements [22].

Fig. 9 also shows the mean values of the measured $[\text{Fe}_i]$ measured on the block with the error bars from 4% uncertainty for the block data [22]. These measured $[\text{Fe}_i]$ values were then corrected based on the doping and τ_{other} values at each point using the error plots presented in Fig. 9 and the Appendix. Both the uncorrected and corrected block data are shown in Fig. 9. We note that the measurement of the interstitial iron concentration on the block when $[\text{Fe}_i] < 10^{11}$ cm^{-3} is subject to less uncertainty than wafer-based measurements, due to the considerably larger volume to surface ratio, as well as the well-defined surface conditions in the block.

After correcting for the effects of nonuniform carrier profiles in the block measurements, and the effects of SiN gettering in the wafer data, the datasets on the block and the wafers are in good agreement. In fact, both corrections are relatively minor. These results confirm that measurements of the dissolved Fe concentration using block lifetime measurements give reliable results under typical measurement conditions for p-type multicrystalline ingots, and can in any case be corrected for the effects of nonuniform injection levels.

V. Conclusion

This paper presents a systematic study on the accuracy of interstitial iron concentrations extracted from QSSPC lifetime measurements on silicon blocks. In general, the QSSPC measurements of $[\text{Fe}_i]$ at the ingot level are subject to only a small error due to the nonuniform carrier profiles in an ingot, and the results were in good agreement with $[\text{Fe}_i]$ measurements on wafers from an adjacent block. The modeling and simulation tool enabled us to validate the accuracy of the interstitial iron concentration measured with the BCT-400 tool. The simulation results showed the error in the extracted interstitial iron concentration is generally less than 20% for $[\text{Fe}_i]$ levels below 10^{11} cm^{-3}, which is typically the case in the central regions of multicrystalline ingots, and can in any case be corrected for.

Appendix

See Fig. 10.

Acknowledgment

References

[1] R. A. Sinton and A. Cuevas, "Contactless determination of current–voltage characteristics and minority-carrier lifetimes in semiconductors from quasi-steady-state photoconductance data," *Appl. Phys. Lett.*, vol. 69, pp. 2510–2512, 1996.

[2] T. Bartel *et al.*, "Dynamics of iron-acceptor-pair formation in co-doped silicon," *Appl. Phys. Lett.*, vol. 103, 2013, Art. no. 202109.

[3] F. Gibaja *et al.*, "Silicon ingot quality and resulting solar cell performance," *Energy Procedia*, vol. 38, pp. 551–560, 2013.

[4] S. Bowden and R. A. Sinton, "Determining lifetime in silicon blocks and wafers with accurate expressions for carrier density," *J. Appl. Phys.*, vol. 102, 2007, Art. no. 124501.

[5] R. Sinton, T. Mankad, S. Bowden, and N. Enjalbert, "Evaluating silicon blocks and ingots with quasi-steady-state lifetime measurements," in *Proc. 19th Eur. Photovolt. Sol. Energy Conf.*, Paris, France, 2004, pp. 520–523.

[6] F. Schindler *et al.*, "Material limits of multicrystalline silicon from state-of-the-art photoluminescence imaging techniques," *Prog. Photovolt.: Res. Appl.*, 2017, to be published.

[7] B. Mitchell, T. Trupke, J. R. W. Weber, and J. R. Nyhus, "Bulk minority carrier lifetimes and doping of silicon bricks from photoluminescence intensity ratios," *J. Appl. Phys.*, vol. 109, 2011, Art. no. 083111.

[8] J. A. Giesecke, R. A. Sinton, M. C. Schubert, S. Riepe, and W. Warta, "Determination of bulk lifetime and surface recombination velocity of silicon ingots from dynamic photoluminescence," *IEEE J. Photovolt.*, vol. 3, no. 4, pp. 1311–1318, Oct. 2013.

[9] S. Herlufsen, K. Bothe, J. Schmidt, R. Brendel, and S. Siegmund, "Dynamic photoluminescence lifetime imaging of multicrystalline silicon bricks," *Sol. Energy Mater. Sol. Cells*, vol. 106, pp. 42–46, 2012.

[10] J. A. Giesecke, M. C. Schubert, F. Schindler, and W. Warta, "Harmonically modulated luminescence: Bridging gaps in carrier lifetime metrology across the PV processing chain," *IEEE J. Photovolt.*, vol. 5, no. 1, pp. 313–319, Jan. 2015.

[11] D. Macdonald, L. Geerligs, and A. Azzizi, "Iron detection in crystalline silicon by carrier lifetime measurements for arbitrary injection and doping," *J. Appl. Phys.*, vol. 95, pp. 1021–1028, 2004.

[12] M. C. Schubert, M. J. Kerler, and W. Warta, "Influence of heterogeneous profiles in carrier density measurements with respect to iron concentration measurements in silicon," *J. Appl. Phys.*, vol. 105, 2009, Art. no. 114903.

[13] A. Cuevas, "Modelling silicon characterisation," *Energy Procedia*, vol. 8, pp. 94–99, 2011.

[14] R. A. Sinton and T. Trupke, "Limitations on dynamic excess carrier lifetime calibration methods," *Prog. Photovolt.: Res. Appl.*, vol. 20, pp. 246–249, 2012.

[15] J. S. Swirhun, R. A. Sinton, M. K. Forsyth, and T. Mankad, "Contactless measurement of minority carrier lifetime in silicon ingots and bricks," *Prog. Photovolt.: Res. Appl.*, vol. 19, pp. 313–319, 2011.

[16] A. Richter, S. W. Glunz, F. Werner, J. Schmidt, and A. Cuevas, "Improved quantitative description of auger recombination in crystalline silicon," *Phys. Rev. B*, vol. 86, 2012, Art. no. 165202.

[17] G. Zoth and W. Bergholz, "A fast, preparation-free method to detect iron in silicon," *J. Appl. Phys.*, vol. 67, pp. 6764–6771, 1990.

[18] D. Macdonald, J. Tan, and T. Trupke, "Imaging interstitial iron concentrations in boron-doped crystalline silicon using photoluminescence," *J. Appl. Phys.*, vol. 103, 2008, Art. no. 073710.

[19] D. Macdonald, T. Roth, P. N. K. Deenapanray, T. Trupke, and R. A. Bardos, "Doping dependence of the carrier lifetime crossover point upon dissociation of iron-boron pairs in crystalline silicon," *Appl. Phys. Lett.*, vol. 89, 2006, Art. no. 142107.

[20] B. Mitchell *et al.*, "Imaging as-grown interstitial iron concentration on boron-doped silicon bricks via spectral photoluminescence," *IEEE J. Photovolt.*, vol. 4, no. 5, pp. 1185–1196, Sep. 2014.

[21] J. Tan, D. Macdonald, F. Rougieux, and A. Cuevas, "Accurate measurement of the formation rate of iron–boron pairs in silicon," *Semicond. Sci. Technol.*, vol. 26, 2011, Art. no. 055019.

[22] A. L. Blum *et al.*, "Interlaboratory study of Eddy-current measurement of excess-carrier recombination lifetime," *IEEE J. Photovolt.*, vol. 4, no. 1, pp. 525–531, Jan. 2014.

[23] A. Y. Liu *et al.*, "Gettering of interstitial iron in silicon by plasma-enhanced chemical vapour deposited silicon nitride films," *J. Appl. Phys.*, vol. 120, 2016, Art. no. 193103.

Authors' photographs and biographies not available at the time of publication.